common edges. Hence, there is no simple relationship between the structures of the title compound and $NaNbS_2$.

The results presented clearly demonstrate the enormous synthetic potential of the reactive flux method. The mild reaction temperatures, at which the polychalcogenide building blocks are retained, together with a large pool of preparative data should enable the inorganic chemist to synthesize new compounds more predictably. This seems to be possible at least for the niobium compounds. In agreement with these assumptions we isolated the first chainlike niobium polyselenide using similar reaction conditions as for the sulfur compounds.[16] Again, its structure is based on $[Nb_2Q_{11}]^{4-}$ units connected through Se_2^{2-} and Se_3^{2-} ligands. It can be expected that many more new and interesting niobium compounds will be accessible by a systematic variation of the reaction conditions.

Received: April 25, 1997
Revised version: September 18, 1997 [Z 10383 IE]
German version: *Angew. Chem.* **1998**, *110*, 140 – 142

Keywords: chain compounds · chalcogens · low-dimensional materials · niobium · reactive melts

[1] S. A. Sunshine, D. Kang, J. A. Ibers, *J. Am. Chem. Soc.* **1987**, *109*, 6202 – 6204.
[2] Reviews: a) M. G. Kanatzidis, A. Sutorik, *Progr. Inorg. Chem.* **1995**, *43*, 151 – 265; b) J. A. Cody, M. F. Mansuetto, S. Chien, J. A. Ibers, *Material Science Forum, Vol. 152 – 153*, Trans Tech Publications, Switzerland, **1994**, 35 – 42.
[3] Selected examples for niobium chalcogenides prepared by the reactive flux method: a) KCu_2NbQ_4 (Q = S, Se): Y.-J. Lu, J. A. Ibers, *J. Solid State Chem.* **1991**, *94*, 381 – 385; b) $K_3Cu_3Nb_2Q_8$ (Q = S, Se): *ibid.* **1992**, *98*, 312 – 317; c) K_2CuNbS_4: W. Bensch, P. Dürichen, C. Weidlich, *Z. Kristallogr.* **1996**, 931; d) $Rb_2AgNbSe_4$: *ibid.* **1996**, 932; e) $K_3Nb_2Se_{11}$: S. Schreiner, L. E. Aleandri, D. Kang, J. A. Ibers, *Inorg. Chem.* **1989**, *28*, 392 – 393.
[4] W. Bensch, P. Dürichen, *Eur. J. Solid State Inorg. Chem.* **1996**, *33*, 527 – 536.
[5] W. Bensch, P. Dürichen, *Z. Anorg. Allg. Chem.* **1996**, *622*, 1963 – 1967.
[6] W. Bensch, P. Dürichen, *Inorg. Chim. Acta* **1997**, *261*, 103 – 107.
[7] W. Bensch, P. Dürichen, *Eur. J. Solid State Inorg. Chem.* **1996**, *33*, 1233 – 1240.
[8] Preparation of $NaNbS_6$: In a dry box Na_2S_3 (2.11 mmol) was mixed with niobium (1.06 mmol) and additional sulfur (4.22 mmol). Na_2S_3 was made by the reaction of stoichiometric amounts of sodium and sulfur in liquid ammonia under an argon atmosphere. The reactants were thoroughly ground together in a mortar and then transferred to a glass ampoule which was subsequently evacuated (10^{-3} mbar) and flame-sealed. The ampoule was heated to 350 °C within 5 h, held at this temperature for 6 d, and cooled to room temperature at a rate of 3 degrees per hour. By washing the resulting melt with DMF and diethyl ether, orange-red, transparent, fiberlike crystals of $NaNbS_6$ were isolated. The homogenity of the product was confirmed by powder X-ray diffraction. All reflections of the powder pattern could be indexed on the basis of $NaNbS_6$. $NaNbS_6$ is stable against air and water.
[9] Crystal structure determination of $NaNbS_6$ ($M_r = 308.26$), orange-red needles, crystal size: $0.05 \times 0.05 \times 1$ mm^3, $a = 7.451(2)$, $b = 12.743(2)$, $c = 7.151(2)$ Å, $\beta = 96.81(1)^\circ$, $V = 674.18$ Å^3 (RT), $\rho_{calcd} = 3.037$ g cm^{-3}, monoclinic, space group Cc (no. 15), $Z = 4$, STOE-AED-II four-circle diffractometer, $Mo_{K\alpha}$ radiation, $\mu = 3.58$ mm^{-1}, 1311 measured reflections in the range $3^\circ < 2\theta < 60^\circ$, 1249 independent reflections used for refinement, structure solution with direct methods (SHELXS-86), structure refinement against F^2 (SHELXL-93), 74 parameters, $w = 1/[\sigma^2(F_o^2) + (0.0235 \cdot P)^2 + 2.88P]$, R for 1224 $F_o > 4\sigma(F_o) = 0.0191$, w$R2$ for all 1249 data = 0.0547, GOF = 1.579, residual electron density: 0.56/ – 0.48 e Å^{-3}. Flack parameter: 0.08(7). All crystals investigated were grown together. For one crystal all 86 reflections found by searching the reciprocal space could be separated into two groups. The reflections in each of these two groups were successfully indexed on the basis of the same monoclinic *C*-centered cell. From the transformation matrix between both individuals, it was shown that all reflections *hk*0 as well as *hk*11 were overlapping. Therefore, a twin refinement with SHELXL-93 was performed. This led to a significantly improved model compared to those obtained only with the raw data (R for all reflections with $F_o > 4\sigma(F_o) = 0.0939$; w$R2 = 0.2887$; residual electron density: 11.60/ – 1.72 e Å^{-3}). Further details of the crystal structure investigation may be obtained from the Fachinformationszentrum Karlsruhe, D-76344 Eggenstein-Leopoldshafen (Germany), on quoting the depository number CSD-407 708.
[10] R. D. Shannon, *Acta Crystallogr. Sect. A* **1976**, *32*, 751 – 767.
[11] UV/Vis diffuse reflectance measurements were carried out on a Leica Orthoplan microscope equipped with a Leica MPV-SP, an ICS quartz UV optic, and a xenon lamp as light source. The resolution was 1 nm, and $BaSO_4$ was used as standard for 100 % reflectance. Absorption data were calculated from the reflectance data using the Kubelka – Munk function.[12] The approximate band gap was determined as the intersection point between the energy axis and the line extrapolated from the linear part of the absorption edge in a $(F(R))^2$ plot.
[12] G. Kortüm, *Reflectance spectroscopy*, Springer, New York, **1969**.
[13] TG/DTA measurements were performed on a SETARAM 92-16 device under N_2.
[14] Additional tempering experiments in glass ampoules produced a yellow solid at the colder end of the ampoule, which was identified as sulfur by X-ray fluorescence analysis (RFA).
[15] W. Omloo, F. Jellinek, *J. Less Common Met.* **1970**, *20*, 121 – 129.
[16] P. Dürichen, M. Bolte, W.Bensch, unpublished results.

Spin Polarization and Ferromagnetism in Two-Dimensional Sheetlike Cobalt(II) Polymers: $[Co(L)_2(NCS)_2]$ (L = Pyrimidine or Pyrazine)**

Francesc Lloret,* Giovanni De Munno,* Miguel Julve, Juan Cano, Rafael Ruiz, and Andrea Caneschi

The spin-polarization mechanism[1] describes how an unpaired electron on one atom polarizes the electron cloud on the adjacent atom in the opposite sense. This would result in an alternation of the spin density at atoms in a bridging unit, and consequently the sign of the magnetic exchange parameter J should alternate at each atom in the bridging unit. In this way, oligocarbenes or radicals linked through *m*-phenyl-

[*] Prof. F. Lloret, Prof. M. Julve, Dr. J. Cano, Dr. R. Ruiz
Departament de Química Inorgànica
Facultat de Química de la Universitat de València
Dr. Moliner 50, E-46100 Burjassot, València (Spain)
Fax: Int. code + (34) 6-386 4322
e-mail: lloret@uv.es

Prof. G. De Munno
Dipartimento di Chimica
Università degli Studi della Calabria
87030 Arcavacata di Rende, Cosenza (Italy)

Dr. A. Caneschi
Dipartimento di Chimica
Università degli Studi di Firenze
75/77 Via Maragliano, I-50144 Firenze (Italy)

[**] This work was supported by the Spanish Dirección General de Investigación Científica y Técnica (DGICYT) (project PB94-1002) and the Italian Ministero dell'Università et della Ricerca Scientifica et Tecnologica. R.R. acknowledges the Spanish Ministery of Education and Science for a postdoctoral fellowship.

  1433-7851/98/3701-0135 $ 17.50+.50/0

enes have been designed with a high-spin ground state and prepared.[2] However, since unpaired electrons have a strong tendency to react and to form covalent bonds, stable high-spin organic materials can be expected to be hard to prepare. In contrast, transition metal ions are very stable spin carriers, and in principle, they would be the best candidates for this purpose. Although the spin polarization was shown to be valid for some oxygen- or nitrogen-containing organic systems[3] as well as for some systems comprising paramagnetic transition metal ions and organic radicals,[4] the limits of its application are unclear, especially for coordination compounds containing transition metal ions as the only spin sources. In fact, the first reports on this topic are not conclusive because the magnetic interactions are weak, and a structural determination is lacking.[5]

In an attempt to verify the validity of the spin-polarization mechanism for these systems, we have prepared the sheetlike polymeric compounds $[CoL_2(NCS)_2]_n$ (**1**, L = pyrazine (pyz); **2**, L = pyrimidine (pym); Figure 1) and studied their variable-

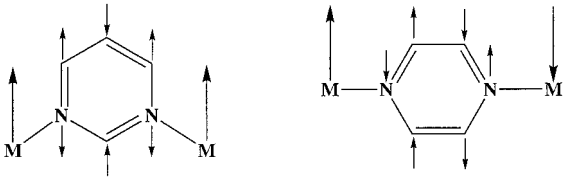

Figure 1. Representation of the spin polarization in pyrimidine (left) and pyrazine ligands (right) bound between two transition metal centers.

temperature magnetic properties. The monomeric complex $[Co(pyd)_4(NCS)_2]$ (**3**, pyd = pyridazine) has been also prepared, and its magnetic properties have been used as a reference for the magnetic behavior of the orbitally degenerate Co^{II} octahedral complex.

The crystal structure of **1**[6] and **2** consists of parallel sheets of square arrays of cobalt atoms bridged by bismonodentate pyz (**1**) or pym (**2**) groups (see Figure 1). A section of the sheetlike structure of **2** is shown in Figure 2. The thiocyanate groups occupy the axial positions. Cobalt is in a compressed octahedral environment with four long Co–N(L) bonds [2.210(1) and 2.261(2) Å for **1** and **2**, respectively] and two short Co–N(NCS) bonds [2.047(2) (**1**) and 2.026(3) Å (**2**)]. The metal atoms in **1** and **2** are on a 2/*m* site; that is, they lie on the inversion center at the intersection of a reflection plane and on a twofold axis perpendicular to it. Within each square of a layer the cobalt atoms lying diagonally opposite each other—Co(1)/Co(1g) and Co(1e)/Co(1f) [for **1** (g) at $x, 1+y, z$, (e) at $-0.5+x, 0.5+y, z$, and (f) at $0.5+x, 0.5+y, z$; for **2** (g) at $1+x, y, z$, (e) at $0.5+x, y, 0.5+z$, and (f) at $0.5+x, y, -0.5+z$]—are generated by a unit cell translation along the *x* and *z* axis for **2** (*x* and *y* axis for **1**). Therefore, the Co(1)···Co(1g) and Co(1e)···Co(1f) distances in **2** are the unit cell values of *a* (9.477(2) Å) and *c* (8.487(2) Å) [*b* (10.383(2) Å and *a* (10.049(2) Å in **1**]. The metal–metal separation through pym in **2** (6.361 Å) is significantly shorter

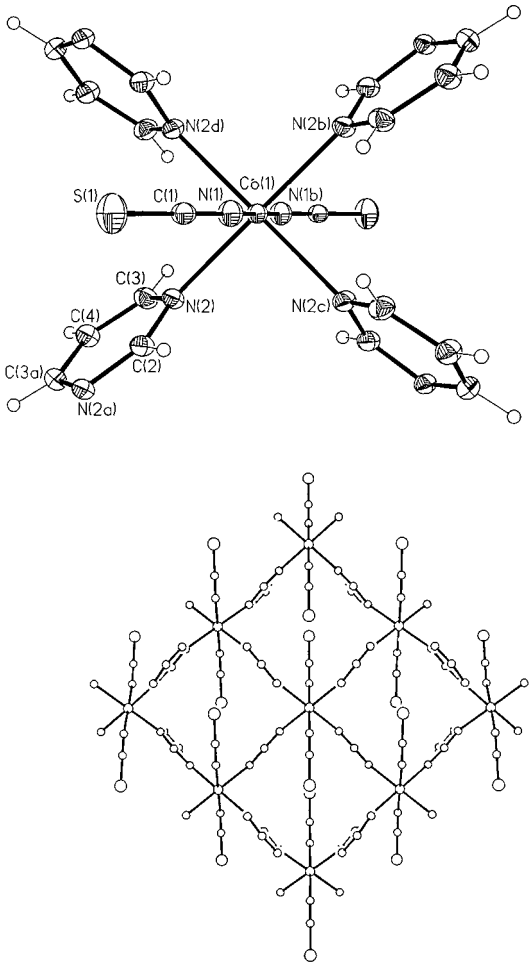

Figure 2. Section of the crystal structure of **2**. Top: Perspective view of the local coordination of the cobalt center (ellipsoids at the 30% probability level). Bottom: View of a sheet along the *xz* plane (hydrogen atoms have been omitted for clarity). Selected bond lengths [Å] and angles [°] with standard deviations in parentheses: Co(1)–N(1) 2.026(3), Co(1)–N(2) 2.261(2); N(1)-Co(1)-N(2) 89.9(1), N(2)-Co(1)-N(1b) 90.1(1), N(2)-Co(1)-N(2c) 91.6(1), N(2)-Co(1)-N(2d) 88.4(1) (generated by symmetry: (b) $-x, -y, -z$; (c) $x, -y, -z$; (d) $-x, y, z$).

than that through pyz in **1** (7.225 Å). Within a square unit of metal atoms in a sheet of **2**, the equatorial planes of opposite Co^{II} ions (constituted by four pyrimidine-nitrogen atoms) are coplanar, whereas the planes of neighboring metal ions form a dihedral angle of 80.7(1)°. The *xz* plane (sheet plane) forms dihedral angles of 40.4(1) and 90.0(1)° with these equatorial planes and with the mean plane of the pym ring, respectively. However, in the case of the related compound **1**, all the equatorial planes of the square unit (ligating atoms are pyrazine-N atoms) are coplanar, and the values of the dihedral angles between the sheet plane (*xy* plane) and the equatorial and mean pyz planes are much reduced [1.5(1) and 65.4(1)°, respectively]. Two adjacent sheets in **2** are separated by 8.487(2) Å (that is, a *b*/2 translation), and they are shifted with respect to the other in such a way that the cobalt atoms of one sheet are located above the centers of the square units of the next sheet. The distance between adjacent layers in **1** is 6.307 Å, and they are related by a translation of *a*/3 along the *x* axis. The shorter interlayer separation in **1** is due to the

  1433-7851/98/3701-0136 $ 17.50+.50/0 *Angew. Chem. Int. Ed.* **1998**, *37*, No. 1/2

greater interpenetration of the axial NCS groups between the sheets that it exhibits. This is impossible in the case of **2**, in which the square units are more puckered and the pym rings are perpendicular to the sheet plane.

The structure of **3** is made up of neutral $[Co(pyd)_4(SCN)_2]$ units (Figure 3). The cobalt is in a compressed octahedral

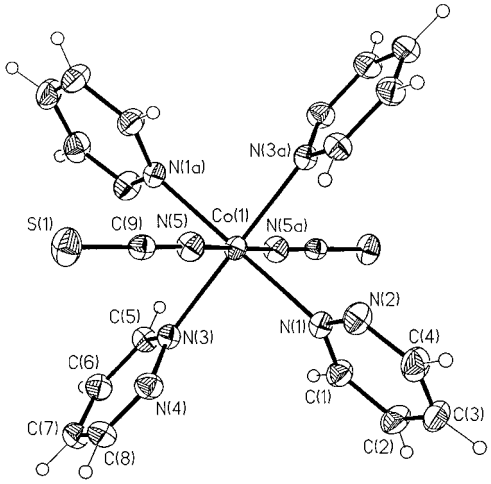

Figure 3. Perspective view of the structure of **3** with thermal ellipsoids at the 30% probability level. Selected bond lengths [Å] and angles [°] with standard deviations in parentheses: Co(1)–N(1) 2.199(2), Co(1)–N(3) 2.208(2), Co(1)–N(5) 2.057(2); N(1)-Co(1)-N(5) 92.9(1), N(1)-Co(1)-N(3) 89.0(1), N(5)-Co(1)-N(3) 90.1(1), N(5)-Co(1)-N(1a) 87.1(1), N(3)-Co(1)-N(1a) 91.0(1), N(3)-Co(1)-N(5a) 89.9(1) (generated by symmetry: (a) $0.5-x, 0.5-y, -z$).

environment with four long Co–N(pyd) bonds [2.199(2)–2.261(2) Å] in the equatorial plane and two short axial Co–(NCS) bonds [2.057(2) Å], as in **1** and **2**. The pyd ligands are planar, and the dihedral angle between the equatorial CoN_4 plane and the pyd ring planes are 50.3(1)° and 120.3(1)°. The shortest intermolecular metal–metal separation is 7.769(3) Å.

The magnetic behavior of **1**–**3** is shown in Figure 4. At room temperature, the $\chi_M T$ value (χ_M is the molar magnetic susceptibility per cobalt atom) is similar for all these

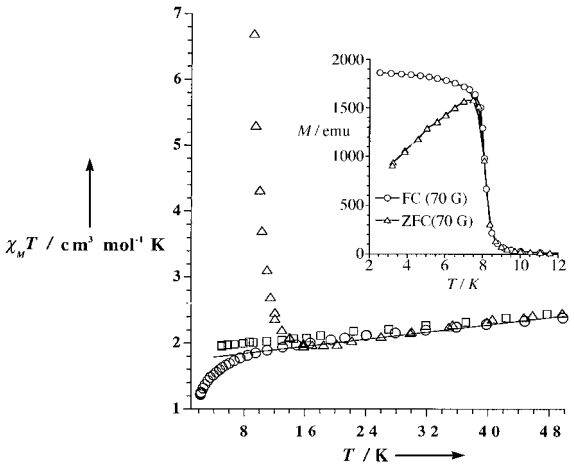

Figure 4. Dependence of the magnetic susceptibility $\chi_M T$ on temperature T for complexes **1** (○), **2** (△), and **3** (□). The inset shows the thermal dependence of the magnetization M in a field of 70 G for **2** after being cooled in an applied field (FC) or in zero field (ZFC).

compounds ($\chi_M T \approx 3.3$ cm³ K mol^{-1}), and it decreases upon cooling. This decrease is related to a spin–orbit coupling effect. In fact, their magnetic behavior can be theoretically modeled, in the temperature range 20–300 K, as monomeric octahedral Co^{II} complexes with λ (spin–orbit coupling parameter) $= -126$ cm^{-1} and κ (orbital reduction parameter) $= 0.75$ (solid line in Figure 4). Complex **3** still follows this theoretical behavior at low temperatures, whereas in the other two cases $\chi_M T$ increases (**2**) or decreases (**1**) rapidly, indicating the presence of ferro- (**2**) and antiferromagnetic (**1**) interactions.

The temperature dependence of the molar magnetization M for **2** was investigated under an applied magnetic field of $H = 70$ G (inset of Figure 4). When the sample was cooled within the field, the field-cooled magnetization showed an abrupt break at 8.2 K. After cooling the sample in zero field and then warming it within the field, the zero-field-cooled magnetization had a maximum just below 8.2 K. All these features are characteristic of a magnetically ordered state below 8.2 K. The ordering temperature T_c was also confirmed by the measurement of both the in-phase (χ') and out-of-phase (χ'') components of the *ac* magnetic susceptibility. The magnetic hysteresis loop for **2** measured at 2.3 K was characteristic of a soft magnet with a small coercive field of 120 G and a remnant magnetization of $0.25\ N\beta$.

The crystal structures of **1** and **2** are thus two important examples of how pyz and pym diazine ligands can spontaneously organize metal ions into a two-dimensional structure and also control the sign of the magnetic interaction in full agreement with the spin-polarization mechanism.

Experimental Section

Synthesis of **1** and **2**: These polymers were prepared in methanol (50 mL) by reaction stoichiometric amounts of $Co(NCS)_2$ and the appropriate diazine (2 mmol). Polymer **1** separates immediately as a polycrystalline orange powder, whereas pink octahedral single crystals of **2** were formed after a few days at room temperature. Prismatic single crystals of **1** were grown by the slow diffusion technique in an H-shaped tube.

Synthesis of **3**: Octahedral orange single crystals of **3** were obtained by slow evaporation (room temperature) of solutions of $Co(NCS)_2$ (1 mmol) and pyd (6 mmol) in methanol (50 mL).

Satisfactory elemental analysis (C,H,N) were obtained for **1**–**3**. Yield about 60%. Crystal structure analyses of **2** and **3**: Siemens R3m/V automatic diffractometer, $Mo_{K\alpha}$, $\lambda = 0.71073$ Å, graphite monochromator, 295 K; data collection, solution, and refinement: $\omega - 2\theta$ scan, standard Patterson methods with subsequent Fourier recycling, SHELXTL-PLUS.[7] **2** ($C_{10}H_8CoN_6S_2$): orthorhombic, space group *Cmca*, $a = 9.477(2)$, $b = 16.284(2)$, $c = 8.487(2)$ Å, $V = 1309.7(4)$ Å^3, $Z = 4$, $\rho_{calcd} = 1.700$ g cm^{-3}, $3 < 2\theta < 55°$, crystal size $0.38 \times 0.21 \times 0.10$ mm; of 811 unique reflections, 661 were assumed observed with $I > 3\sigma(I)$; refinement of 51 variables with anisotropic thermal parameters for all non-hydrogen atoms gave $R = 0.028$, $R_w = 0.031$ and $S = 1.22$. **3** ($C_{18}H_{16}CoN_{10}S_2$): monoclinic, space group *C2c*, $a = 12.341(5)$, $b = 12.950(5)$, $c = 14.322(5)$ Å, $\beta = 109.21(3)°$, $V = 2161(1)$ Å^3, $Z = 4$, $\rho_{calcd} = 1.523$ g cm^{-3}, $3 < 2\theta < 54°$, crystal size $0.42 \times 0.37 \times 0.32$ mm; of 2380 unique reflections, 1924 were assumed observed with $I > 3\sigma(I)$; refinement of 142 variables with anisotropic thermal parameters for all non-hydrogen atoms gave $R = 0.031$, $R_w = 0.038$ and $S = 1.23$. Crystallographic data (excluding structure factors) for the structures reported in this paper have been deposited with the Cambridge Crystallographic Data centre as supplementary publication no. CCDC-100411. Copies of the data can be obtained free of charge on application to

CCDC, 12 Union Road, Cambridge CB21EZ, UK (fax: int. code + (44) 1223-336033; e-mail: deposit@chemcrys.cam.ac.uk).

Received: June 9, 1997
Supplemented version: September 26, 1997 [Z10521IE]
German version: *Angew. Chem.* **1998**, *110*, 143 – 145

Keywords: cobalt · layered compounds · magnetic properties · N ligands · spin polarization

[1] a) H. M. McConnell, *J. Chem. Phys.* **1963**, *39*, 1910; b) N. Mataga, *Theor. Chim. Acta* **1968**, *10*, 372; c) O. Kahn, *Molecular Magnetism*, VCH, New York, **1993**.
[2] H. Iwamura, *Adv. Phys. Org. Chem*. **1990**, *26*, 179.
[3] a) F. Kanno, K. Inoue, N. Koga, H. Iwamura, *J. Phys. Chem*. **1993**, *97*, 13267; b) M. Kitano, Y. Ishimaru, K. Inoue, N. Koga, H. Iwamura, *Inorg. Chem*. **1994**, *33*, 6012.
[4] N. Koga, H. Ishimanu, H: Iwamura, *Angew. Chem.* **1996**, *108*, 815; *Angew. Chem. Int. Ed. Engl.* **1996**, *35*, 755, and references therein.
[5] a) H. Oshio, *J. Chem. Soc. Chem. Commun*. **1991**, 240; b) A. M. W. Cargill Thompson, D. Gatteschi, J. A. McCleverty, J. A. Navas, E. Rentschler, M. D. Ward, *Inorg. Chem*. **1996**, *35*, 2701.
[6] During the preparation of this manuscript the structure of **1** was published (J. Lu, T. Paliwala, S. C. Lim, C. Yu, T. Niu, A. J. Jacobson, *Inorg. Chem.* **1997**, *36*, 923). Because our structural data of **1** fully agree with that reported, we have quoted only a few pertinent structural data of **1** for comparison with that of **2**.
[7] SHELXTL-PLUS Version 4.21/V: Siemens Analytical X-Ray Instruments Inc., Madison, WI (USA), **1990**.

Synthetic *Shigella* Vaccines: A Carbohydrate – Protein Conjugate with Totally Synthetic Hexadecasaccharide Haptens**

Vince Pozsgay*

Carbohydrate-based antibacterial vaccines are among the most successful carbohydrate pharmaceuticals.[1] The basis of using carbohydrates as vaccine components is that the capsular polysaccharides (CPs) and the O-specific polysaccharides (O-SPs) on the surface of pathogenic bacteria are both essential virulence factors and protective antigens, and that serum antibodies raised against these polysaccharides may provide immunity by killing the inoculum.[1] This principle led to the development of CP vaccines against Pneumococci and other Gram-positive bacteria. The inability of polysaccharides to elicit protective levels of anti-carbohydrate antibodies in infants could be overcome by their covalent attachment to proteins that conferred T-cell dependent properties.[2] This principle led to the construction of vaccines against *Haemophilus influenzae* b (Hib),[3] and in countries where these vaccines are routinely used, meningitis and other diseases caused by Hib have been virtually eliminated.[4] Extension of the conjugate technology to the O-SPs of Gram-negative bacteria provided a new generation of glycoconjugate vaccines that are undergoing various phases of clinical trials.[5]

While the immunogenicity and the efficacy of the glycoconjugate vaccines are established, their structural requirements are not well defined. Further improvement of the immunologic properties of conjugate vaccines requires the knowledge of the optimal size of the saccharide, the preferred method of its attachment to the protein, and the saccharide/protein ratio necessary for optimal immunogenicity. Success in this area will depend on the availability of well-defined saccharides that are representative of the native polysaccharides.[6]

Here we describe our approach to a hexadecasaccharide fragment[7] of the O-SP (**A**) of *Shigella dysenteriae* type 1,[8] a human pathogen that is a major causative organism of endemic and epidemic dysentery worldwide.[9]

→3)-α-L-Rha*p*-(1→2)-α-D-Gal*p*-(1→3)-α-D-Glc*p*NAc-(1→3)-α-L-Rha*p*-(1→
A

The target saccharide is equipped with a spacer as the aglycon portion. A heterobifunctional linker unit was appended to this end of the saccharide assembly for covalent attachment to human serum albumin (HSA) as a model carrier protein. The single-point attachment leaves the entire saccharide chain available for interaction with B cell receptors. The average number of saccharide chains attached to HSA is defined by matrix-assisted laser desorption ionization time of flight (MALDI-TOF) mass spectrometry.

The overall strategy to the target **21** (see below) called for the assembly of a tetrasaccharide repeating unit (**12**, **14,** see Scheme 1) in a form that may be used in an iterative fashion for blockwise construction of higher oligosaccharides.[10] In this endeavor we relied on our previous experience in synthesizing related compounds.[7, 11] Of particular importance was the realization that for the iterative building of a saccharide of this size, the tetrasaccharide frame along the polysaccharide chain should correspond to that shown by formula **A**. We also found that

1) the tetrasaccharide block can be most conveniently assembled in a stepwise fashion,
2) the Gal and the Rha synthons should be installed in a prefabricated form which allows the attachment of the subsequent residue after only one deprotecting step, and that
3) the use of a prefabricated synthon for the GlcN unit has no advantage on the overall yield.

Furthermore, we concluded that intermediates with multiple azide groups should be avoided because of the difficulties that may arise in their conversion to acetamido functions.[12]

The principles established in previous studies led to the selection of four monosaccharide building blocks **1**, **2**, **7**, and **11** that were prepared as reported for related synthons.[7, 11, 13] The assembly of the tetrasaccharide **12** started with the condensation of the rhamnose derivative **1** with the chloride **2** (Scheme 1, Table 1). The nonparticipating azido group of **2**

[*] Dr. V. Pozsgay
Laboratory of Developmental and Molecular Immunity
National Institute of Child Health and Human Development
National Institutes of Health
6 Center Drive MSC 2720, Bethesda, MD 20892-2720 (USA)
Fax: Int. code + (1) 301 402-9108
e-mail: vipo@helix.nih.gov

[**] The author thanks Dr. John B. Robbins and Dr. Rachel Schneerson for many stimulating discussions. Dr. Lewis Pannell and Noel Whittaker are thanked for recording the mass spectra.

  1433-7851/98/3701-0138 $ 17.50+.50/0